Solar Physics
DOI: 10.1007/•••••-•••-•••-••••-•

Line-of-sight observables algorithms for the *Helioseismic and Magnetic Imager* (HMI) Instrument tested with *Interferometric BI-dimensional Spectrometer* (IBIS) observations

Sébastien Couvidat[1] · **S. P. Rajaguru**[2] · **Richard Wachter**[1] · **K. Sankarasubramanian**[3] · **Jesper Schou**[1] · **Philip H. Scherrer**[1]

Received: 11 October 2011

Abstract The *Helioseismic and Magnetic Imager* (HMI) instrument onboard the *Solar Dynamics Observatory* produces line-of-sight observables (Doppler velocity, magnetic-field strength, Fe I linewidth, linedepth, and continuum intensity) as well as vector-magnetic-field maps at the solar surface. The accuracy of line-of-sight observables is dependent on the algorithm used to translate a sequence of HMI filtergrams into the corresponding observables. Using one hour of high-cadence imaging spectropolarimetric observations of a sunspot in the Fe I line at 6173 Å through the *Interferometric BI-dimensional Spectrometer* installed at the Dunn Solar Telescope, and the Milne-Eddington inversion of the corresponding Stokes vectors, we test the accuracy of the observables algorithm currently implemented in the HMI pipeline at Stanford University: the MDI-like algorithm. We also compare this algorithm to others that may be implemented in the future in an attempt at improving the accuracy of HMI observables: a least-squares fit with a Gaussian profile, a least-squares fit with a Voigt profile, and the use of second Fourier coefficients in the MDI-like algorithm.

Keywords: Sun: helioseismology, Instrument: SDO/HMI, IBIS

1. Introduction

The *Helioseismic and Magnetic Imager* instrument (HMI; Schou *et al.*, 2011) onboard the *Solar Dynamics Observatory* satellite (SDO) makes measurements, in the absorption line Fe I centered at the in-air wavelength 6173.3433 Å (*e.g.*

[1] W.W. Hansen Experimental Physics Laboratory, Stanford University, USA
email: couvidat@stanford.edu
[2] Indian Institute of Astrophysics, Bangaluru, India
[3] Space Astronomy Group, ISRO satellite Centre, Bengaluru, India; and Indian Institute of Astrophysics, Bangaluru, India

Dravins, Lindegren, and Nordlund, 1981; Norton *et al.*, 2006), of the motion of the solar photosphere to study solar oscillations, and of the polarization to study all three components of the photospheric magnetic field. HMI samples the neutral iron line at six positions (wavelengths) symmetrical around the line center at rest. Line-Of-Sight (LOS) observables are produced every 45 s and are: Doppler velocity at the solar surface, LOS magnetic-field strength, Fe I linewidth, linedepth, and continuum intensity. They are calculated using 12 filtergrams: images taken at six wavelengths and two polarizations (Left-Circular and Right-Circular Polarizations, hereafter LCP and RCP). Unlike the *Michelson Doppler Imager* (MDI) instrument (Scherrer et *al.*, 1995) on which HMI is based, the observables calculations are performed on the ground at Stanford University, and not on board the satellite. This allows for more flexibility regarding which algorithm to apply, and makes reprocessing possible in the eventuality that a better algorithm is later implemented.

On June 8, 2007, the sunspot NOAA AR10960 was observed by the *Interferometric BI-dimensional Spectrometer* (IBIS) instrument (Cavallini, 2006) installed at the Dunn Solar Telescope of the National Solar Observatory in Sacramento Peak (New Mexico, USA). The full Stokes profile (I,Q,U, and V) of the Fe I line was scanned and imaged for 7 h at a cadence of 47.5 s, close to the HMI cadence (see Rajaguru et *al.*, 2010, for details on these IBIS data processing and calibration). The IBIS images have a spectral resolution of ≈ 25 mÅ and an image scale of 0.165" (both three times better than HMI), and the Fe I line was sampled at 23 different wavelengths spanning ≈ 900 mÅ. We select the first observation hour, to keep only the best seeing interval and to match the time interval selected for the Milne-Eddington inversion of the Stokes vectors (inversion following the method described in Skumanich and Lites, 1987).

The IBIS observations present some advantages over the HMI ones resulting from a higher number of wavelength samples. This allows for an interpolation of the line profiles at each pixel on a finer wavelength grid: simulations of HMI intensities can therefore be obtained by applying the filter transmission profiles to these wavelength-interpolated lines, and the accuracy of the LOS observables returned by the MDI-like algorithm can be investigated. Other algorithms can also be studied, e.g. a least-squares fit with an appropriate Fe I profile. Moreover the Sun-Earth radial velocity varied little during the IBIS observation timespan (from -120.98 m s^{-1} to -95.43 m s^{-1} during the first observation hour, compared to a 358 m s^{-1} change for the HMI-Sun radial velocity over the same time interval on June 8, 2011). Another consideration for using IBIS data and their Milne-Eddington inversion is that, at the time of writing, the full Stokes-vector inversions of HMI have not yet been officially released: the inversion code (vfisv; Borrero *et al.*, 2010) is still being fine-tuned. However, among others, IBIS spatial resolution is different from HMI, a fact that needs to be factored in when interpreting the results: mainly due to convective blueshift (depending on how well granules are resolved), a different spatial resolution translates into a different Fe I line profile. In Section 2 we describe the MDI-like algorithm implemented in the HMI pipeline, in Section 3 we describe other algorithms tested, and in Section 4 we introduce the IBIS data used. We present the results in Section 5 and we conclude in Section 6.

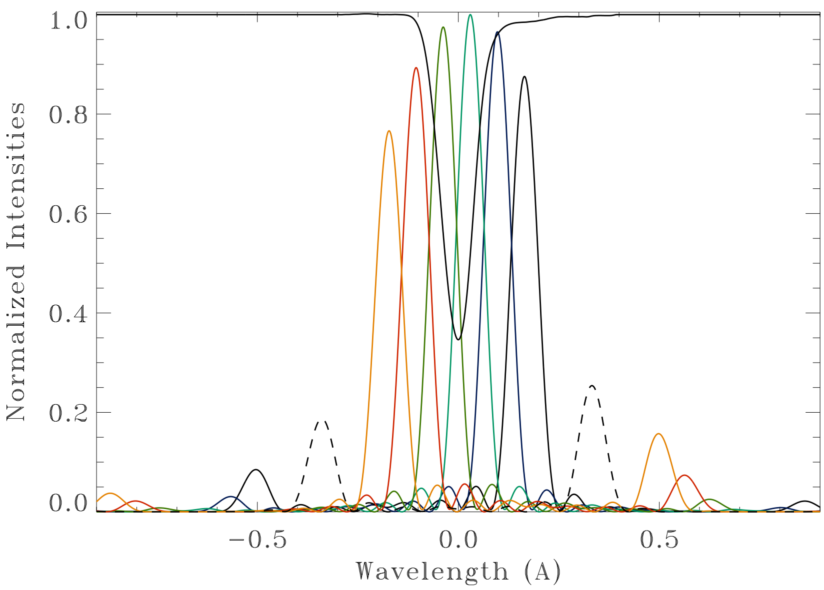

Figure 1. Example of HMI-filter transmission profiles obtained from calibration procedures (from Couvidat et *al.*, 2011). Six tuning positions are shown with respect to the Fe I solar line (black line) at disk center and at rest, on top of a continuum tuning position (dashed line). The Fe I line profile was provided by R. K. Ulrich (*private communication*) and obtained at the Mount Wilson Observatory.

2. MDI-like Algorithm

This algorithm is based on what was implemented for the SOHO/MDI instrument. It combines filtergrams taken at 6 wavelengths. The profiles of the corresponding HMI filter transmittances need to be accurately known. The HMI optical-filter system is composed of a front window, a blocking filter, a five-stage Lyot filter, and two Michelson interferometers. The Lyot element E1 (element with the lowest FWHM) and the two interferometers are tunable, allowing for the taking of filtergrams at different wavelengths. The calculation of the resulting transmission profiles is detailed in Couvidat et *al.* (2011). An example is reproduced on Figure 1. The profiles slowly change with time and vary somewhat across the HMI CCDs.

2.1. Theoretical algorithm

The MDI-like algorithm starts with a calculation of the first and second Fourier coefficients a_n and b_n of the Fe I line profile $I(\lambda)$ (λ is the wavelength):

$$a_1 = \frac{2}{T}\int_{-\frac{T}{2}}^{+\frac{T}{2}} I(\lambda)\cos\left(2\pi\frac{\lambda}{T}\right)d\lambda \; ; \; b_1 = \frac{2}{T}\int_{-\frac{T}{2}}^{+\frac{T}{2}} I(\lambda)\sin\left(2\pi\frac{\lambda}{T}\right)d\lambda \qquad (1)$$

$$a_2 = \frac{2}{T}\int_{-\frac{T}{2}}^{+\frac{T}{2}} I(\lambda)\cos\left(4\pi\frac{\lambda}{T}\right)d\lambda \; ; \; b_2 = \frac{2}{T}\int_{-\frac{T}{2}}^{+\frac{T}{2}} I(\lambda)\sin\left(4\pi\frac{\lambda}{T}\right)d\lambda \qquad (2)$$

where T is the "period" of the observation wavelength span, nominally $T = 6 \times 68.8 = 412.8$ mÅ (i.e. 6 times the nominal separation between two filters). MDI was designed so that the FWHM of its filter transmission profiles matches the FWHM of the Ni I line, and the four — equally spaced — wavelength samples cover a period equal to twice this FWHM. Consequently with MDI, and unlike HMI, nearly all the spectral power in the solar line is captured by the first Fourier coefficients. HMI was not designed this way because the dynamic range corresponding to twice the FWHM of the Fe I line is too small to accommodate the large velocity variations resulting from the SDO orbit.

Assuming that the "pure" solar line, i.e. prior to its convolution by the HMI filter profiles, is a Gaussian:

$$I(\lambda) = I_c - I_d \exp\left[-\frac{(\lambda-\lambda_0)^2}{\sigma^2}\right] \qquad (3)$$

where I_c is the continuum intensity, I_d is the linedepth, λ_0 is the Doppler shift, and σ is a measure of the linewidth (FWHM$= 2\sqrt{\ln(2)}\,\sigma$), the Doppler velocity v can be expressed as:

$$v = \frac{dv}{d\lambda}\frac{T}{2\pi}\,\mathrm{atan}\left(\frac{b_1}{a_1}\right) \qquad (4)$$

with $dv/d\lambda = 299792458.0\ \mathrm{m\,s^{-1}}/6173.3433$ Å$= 48562.4\ \mathrm{m\,s^{-1}}$ Å^{-1}. The second Fourier coefficients could also be used:

$$v_2 = \frac{dv}{d\lambda}\frac{T}{4\pi}\,\mathrm{atan}\left(\frac{b_2}{a_2}\right) \qquad (5)$$

The linedepth I_d is equal to:

$$I_d = \frac{T}{2\sigma\sqrt{\pi}}\sqrt{a_1^2+b_1^2}\,\exp\left(\frac{\pi^2\sigma^2}{T^2}\right) \qquad (6)$$

while σ is equal to:

$$\sigma = \frac{T}{\pi\sqrt{6}}\sqrt{\mathrm{alog}\left(\frac{a_1^2+b_1^2}{a_2^2+b_2^2}\right)} \qquad (7)$$

HMI samples the iron line at six points and therefore only discrete approximations to the Fourier coefficients can be calculated, for instance:

$$a_1 \approx \frac{2}{6}\sum_{j=0}^{5} I_j \cos\left(2\pi\frac{2.5-j}{6}\right) \qquad (8)$$

The b_n are determined by a similar formula with cosine replaced by sine. These a_n and b_n are calculated separately for the LCP and RCP polarizations. Applying Equation (4) produces two velocities: v_{LCP} and v_{RCP}.

The "pure" Fe I line is not a Gaussian and the discrete approximations to a_n and b_n are not accurate due to a reduced number of sampling points and because the filter profiles are not delta functions (consequently the observables calculated are relative to the Fe I line convolved by the filters, not the "pure" line). Therefore, $v_{\rm LCP}$ and $v_{\rm RCP}$ need to be corrected. Look-up tables obtained from a realistic model of the "pure" Fe I line at rest are used for this purpose. The line profile is shifted in wavelength to simulate a Doppler velocity. At each shift, the profile is convolved by the filter transmittances. The MDI-like algorithm is then applied to the simulated HMI intensities. The velocity returned by the algorithm is a function of the actual (input) Doppler velocity. The inverse function is called a look-up table (a misnomer that is a legacy of the MDI implementation). The tables vary across the HMI CCDs. They are linearly interpolated at $v_{\rm LCP}$ and $v_{\rm RCP}$ to derive corrected Doppler velocities $V_{\rm LCP}$ and $V_{\rm RCP}$. In the rest of this paper, 1st Fourier-coefficient MDI-like algorithm refers to the use of a_1 and b_1 to estimate the Doppler velocities and their subsequent correction with look-up tables.

Calibration of the HMI filters shows some residual errors (at the percent level) on their transmittances, resulting in imperfect look-up tables. Conversely, the SDO orbital velocity is known very accurately and can be used to, partly, improve these tables. This additional step is implemented in the HMI pipeline, but will be ignored here.

Finally, the $V_{\rm LCP}$ and $V_{\rm RCP}$ velocities are combined to produce a Doppler-velocity estimate V:

$$V = \frac{V_{\rm LCP} + V_{\rm RCP}}{2} \tag{9}$$

while the LOS magnetic-field strength B is:

$$B = (V_{\rm LCP} - V_{\rm RCP}) K_m \tag{10}$$

where $K_m = 1.0/(2.0 \times 4.67 \cdot 10^{-5}\, \lambda_0\, g_L\, c) = 0.231$ G m^{-1} s, $g_L = 2.5$ (Norton *et al.*, 2006) is the Landé g-factor, and c is the speed of light.

An estimate of the continuum intensity I_c is obtained by reconstructing the solar line from the Doppler-shift, linewidth, and linedepth estimates:

$$I_c \approx \frac{1}{6} \sum_{j=0}^{5} \left[I_j + I_d \exp\left(-\frac{(\lambda_j - \lambda_0)^2}{\sigma^2} \right) \right] \tag{11}$$

where λ_0, I_d, and σ are the values retrieved by Eqs (4), (6), and (7), and λ_j are the nominal wavelengths corresponding to each filter profile.

2.2. Actual implementation

The algorithm is implemented slightly differently in the HMI pipeline. Tests on artificial Gaussian lines and using the proper HMI filter transmittances showed that the theoretical algorithm overestimates the linewidth of "pure" Gaussian lines by $\approx 20\%$ for a line with $I_d = 0.62$ and $\sigma = 0.0613$ Å (values in Norton *et al.*, 2006). Conversely, the linedepth is underestimated by $\approx 33\%$. The continuum intensity seems only slightly underestimated (by $\approx 1\%$). These errors on the parameters of artificial Gaussian lines arise because the number of wavelength samples is too small and the filters are not delta functions.

Due to an initial error in implementation, a factor $K_1 = 5/6$ multiplies σ returned by Equation (7), while a factor $K_2 = 6/5$ multiplies I_d returned by Equation (6). The integral of a Gaussian is proportional to $I_d\,\sigma$: therefore, multiplying these two quantities by K_1 and $K_2 = 1/K_1$ keeps the integral constant and produces a same continuum intensity with Equation (11). In the current implementation, the linedepths and linewidths returned by Eqs (6) and (7) are still intentionally multiplied by K_2 and K_1, respectively, so that both values are expected to be closer to the actual ones, while the continuum intensity remains unchanged. In the rest of the paper, we only consider linewidths and linedepths corrected by K_1 and K_2 when refering to the MDI-like algorithm.

Finally, when computing linedepth and continuum intensity with Eqs (6) and (11), the σ used in these equations is not the one derived from Equation (7) and that is saved in the observables series. A 5-order polynomial was fitted to an azimuthal average (about the solar disk center) of an HMI linewidth map obtained from Equation (7) (and corrected by K_1) during a period of low solar activity, as a function of center-to-limb distance. Linewidths calculated from this polynomial are used instead of those from Equation (7) because the latter sometimes returns spurious values in presence of locally strong magnetic fields, especially for pixels away from solar disk center.

3. Other Observables Algorithms Tested

Algorithms other than the MDI-like one based on a_1 and b_1 are also applied to IBIS data: a MDI-like algorithm with the 2nd Fourier coefficients, a least-squares fit with a Gaussian profile for the Fe I line, and a least-squares fit with a Voigt profile.

Before the launch of SDO it was considered to average results of both the first and second Fourier coefficients when computing Doppler velocity and field strength, and to later transition to a least-squares fit. The second Fourier coefficients have half the dynamic range of a_1 and b_1, but the latter are used to properly offset the velocity v_2 (returned by a_2 and b_2) by the required amount when v (returned by a_1 and b_1) is outside the dynamic range of a_2 and b_2. Using the 2nd Fourier coefficients turned out to be more difficult than anticipated: there was a significant number of saturated pixels where the magnetic field is strong, and the velocities calculated differed significantly from the 1st Fourier-coefficient ones. Due to tight time constraints it was decided to postpone the implementation of the second Fourier-coefficients algorithm. Therefore, only half the information available is utilized and the rms variation on Doppler velocity due to photon noise is larger. A possible improvement to the HMI pipeline would be to include these second Fourier coefficients: the impact is discussed here.

The MDI-like algorithm is computationally very fast: no fit is involved, only a combination of six wavelengths followed by a linear interpolation. That is one reason this algorithm was preferred over least-squares fits for the time being. However, the look-up tables are computed for a reference Fe I profile in the quiet Sun and therefore the algorithm is expected to fare poorly in regions of strong magnetic fields. Conversely, a least-squares fit with a reasonable model of the Fe I line is expected to provide more accurate results, because the profile is adjusted in depth and width during the fit to reflect the presence of magnetic fields. The simplest model of Fe I line used here is a Gaussian, resulting from Doppler broadening alone: it is a poor approximation to the iron line. A more elaborate model is the Voigt profile: a convolution between a Gaussian profile (thermal broadening) and a Lorentzian profile (produced by radiative and collisional broadenings). It is more representative of the actual Fe I line, even though it is symmetrical around the central wavelength while the solar line displays a significant asymmetry. The Voigt profile implemented is characterized by five quantities: a Doppler shift λ_0, a linewidth σ of the Gaussian part of the profile, a continuum intensity I_c, a scale parameter I_d related to the linedepth, and a damping parameter a. Least-squares fits of three observed Fe I line profiles provided by R. Ulrich (*private communication*) at different solar center-to-limb distances and obtained at Mount Wilson Observatory return values for a in the range $0.16 - 0.2$, while fits on Kitt-Peak Atlas data return $a = 0.25$. This is close to the $a = 0.23$ quoted by Bell and Meltzer (1959). Here we set $a = 0.225$, but the exact value has little impact on the conclusions of this paper (we tested lower values).

4. IBIS Data

Rajaguru *et al.* (2010) detail the IBIS data and Milne-Eddington (M-E) inversion utilized here. The first hour of observation is selected, corresponding to the best seeing interval. The initial datacube format is $512 \times 512 \times 23 \times 4 \times 79$, where the first two dimensions refer to the Cartesian coordinates on the CCD (the original 1024×1024 IBIS data were rebinned by a factor 2), the next dimensions are the number of wavelength samples (23) and of Stokes parameters (4), and the last dimension is the number of time steps (the datacube spans 1.03 hours at a cadence of 47.5 s). To compare the LOS magnetic-field strength returned by the observables algorithms with the result of the M-E inversion of the Stokes vector, we follow Rajaguru *et al.* (2010) and select a 341×341 pixel region centered on the sunspot. The M-E inversion in Rajaguru *et al.* (2010) was performed on a one-hour temporal average of the data to reduce the noise level: therefore we also average the datacube over one hour, despite the smoothing of the line profiles such averaging produces. We only consider the LCP (I+V) and RCP (I−V) polarizations. The final datacube contains $341 \times 341 \times 23 \times 2$ points. At each pixel, a cubic spline interpolation is applied (a quadratic interpolation was also tested) of the 23 wavelength samples, to obtain LCP and RCP profiles on a finer wavelength grid with a sampling rate of 0.5 mÅ.

Figure 2 shows maps of the LOS observables for the temporally-averaged IBIS data, obtained with the 1st Fourier-coefficients MDI-like algorithm. The square window centered on the sunspot shows the area selected for various plots

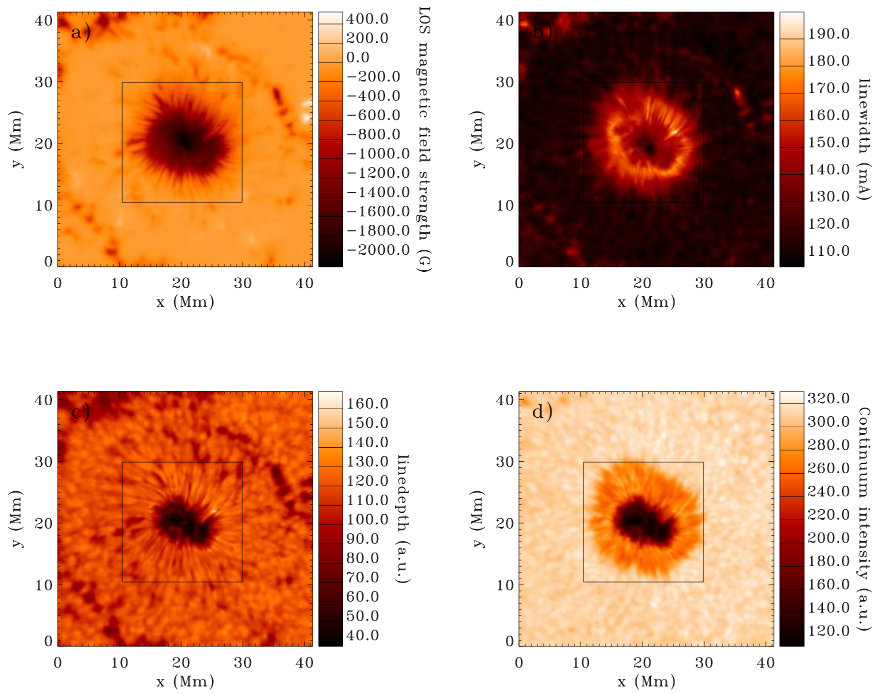

Figure 2. Situation maps showing the LOS observables obtained with the 1st-Fourier coefficient MDI-like algorithm. a) magnetic field strength (the color scale is truncated); b) linewidth; c) linedepth; d) continuum intensity. The active region NOAA AR10960 was observed by the IBIS instrument on June 8, 2007. The square window centered on the sunspot shows which pixels were selected for various figures of Section 5.

of Section 5: outside this window the M-E inversion is very noisy due to low polarization signal. No attempt was made to correct for scattered light on IBIS observations: therefore, the signal in the sunspot umbra partly comes from adjacent areas and especially from the penumbra. The M-E inversion was performed on the raw IBIS line profiles, i.e. no deconvolution by the IBIS filter profiles was attempted because the profiles were not available at the time the inversion was made. A deconvolution of a typical IBIS Stokes-I profile by a Gaussian with a FWHM = 25 mÅ produces a deconvolved line close to the original one (the FWHM is reduced by only $\approx 2.5\%$ while the linedepth is increased by a similar amount). Therefore, using spectrally convolved lines instead of deconvolved ones should have little impact on the conclusions of this paper.

5. Results

To simulate the 12 HMI filtergrams needed to derive LOS observables, a set of HMI filter transmission profiles obtained from calibration procedures and valid

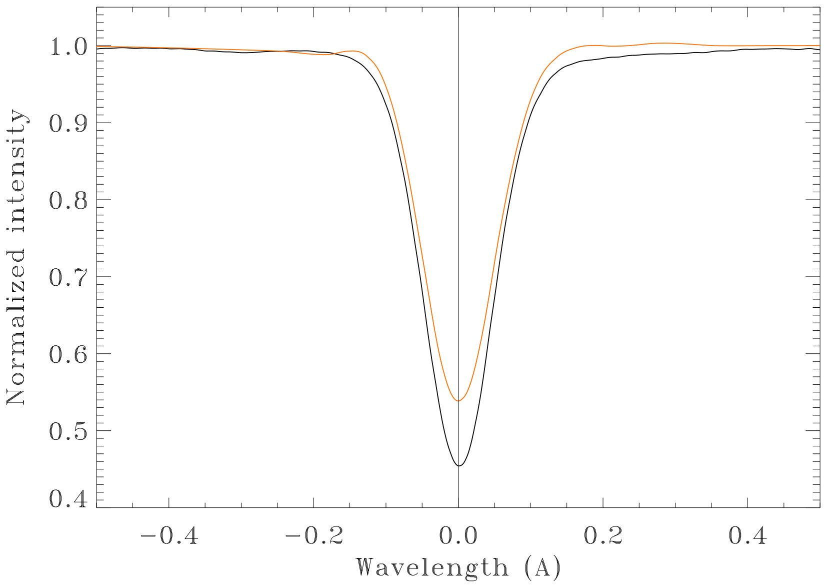

Figure 3. Comparison of Fe I line profiles: the black solid line is from the Kitt Peak atlas obtained at the Kitt Peak-McMath Pierce telescope, while the solid orange line is the reference profile used here to calculate look-up tables for the MDI-like algorithms and obtained from an hour-long average of IBIS data in a quiet-Sun pixel.

at solar disk center is used. The temporally-averaged wavelength-interpolated LCP and RCP IBIS profiles are convolved by the filter profiles, resulting in simulated HMI intensities.

The look-up tables required by MDI-like algorithms necessitate a reference Fe I line, usually taken at rest: therefore a Stokes I profile is selected, for which the I+V and I−V components superimpose (denoting the absence of any significant magnetic field). The resulting line is shown on Figure 3. The magnetic field strength is negligible at several locations in the IBIS field of view, and several reference profiles were tested: despite minor differences, our conclusions are unaffected by a specific choice. The reference profile selected is broader (with a FWHM of 116.8 mÅ instead of 102 mÅ) and shallower (with a linedepth of 0.461 instead of 0.66) than the line parameters reported by Norton *et al.* (2006): the difference mainly comes from the temporal averaging of IBIS data, the difference in spatial resolution, and to a lesser extent from the convolution of the IBIS line by the instrumental transmittance and the presence of instrumental scattered light.

5.1. Doppler velocity and LOS magnetic-field strength

Figure 4 displays the Doppler velocity and LOS magnetic-field strength returned by different observables algorithms. It is a cut at the latitude crossing the center of the sunspot. The average velocity returned by each algorithm in

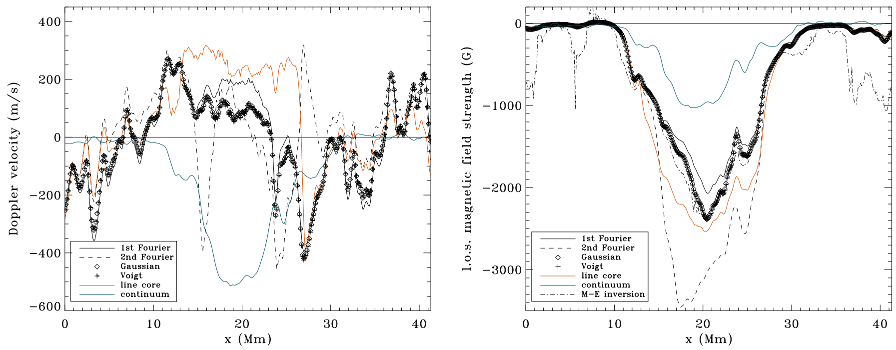

Figure 4. Doppler velocities (left panel) and LOS magnetic-field strengths (right panel) returned by various observables algorithms. This is a cut at the latitude crossing the center of the sunspot. The curve labeled "continuum" shows a normalized continuum intensity, for comparison purpose. On the left panel, the average velocity in the quiet Sun returned by each algorithm has been subtracted.

Table 1. Pearson linear correlation coefficients between Doppler velocities returned by different algorithms for the pixels located in the square window of Figure 2.

	1st Fourier	2nd Fourier	Gauss	Voigt	line core
1st Fourier	100.0	35.0	99.4	99.3	79.5
2nd Fourier	35.0	100.0	37.8	37.8	24.6
Gauss	99.4	37.8	100.0	99.9	77.6
Voigt	99.3	37.8	99.9	100.0	77.5
line core	79.5	24.6	77.6	77.5	100.0

a nearby quiet-Sun region has been subtracted to facilitate comparisons. The curves labeled "line core" show velocity and field strength obtained by locating the minimum of the interpolated Fe I profiles: once the approximate location is known, a second-order polynomial fit is performed in the wavelength range [-25,+25] mÅ around this location, to determine the exact minimum location. Line-core velocities are not expected to match other algorithms' velocities: e.g., Fleck, Couvidat, and Strauss (2011) showed that the MDI-like algorithm based on a_1 and b_1 does not track the Doppler shift of the core of the line but rather of its center of gravity, as expected. Other algorithms are sensitive to different parts of the Fe I line, corresponding to different atmospheric heights. In the sunspot, the MDI-like algorithm with a_1 and b_1 returns velocities that are larger than the least-squares fits ones, by up to 300 m s^{-1}, with an average difference of about 90 m s^{-1} in the umbra. In the quiet Sun all the velocities are similar (due to the subtraction of the respective averages). Table 1 lists the linear (Pearson) correlation coefficients between velocities returned by different algorithms. The lowest correlation is obtained between 2nd Fourier-coefficients MDI-like algorithm and line-core velocities.

Table 2. Standard deviation (in m s^{-1}) of Doppler velocity retrieved by the LOS algorithms and resulting from photon noise, for three different Doppler velocities.

velocity (m s^{-1})	1st Fourier	2nd Fourier	Gauss	Voigt
−2016	19.18	32.48	15.66	15.76
0	19.17	29.24	14.96	14.80
+2016	19.35	30.45	15.80	15.98

Table 3. Pearson linear correlation coefficients between LOS magnetic-field strengths returned by different algorithms for the pixels located in the square window of Figure 2.

	1st Fourier	2nd Fourier	Gauss	Voigt	M-E LOS field
1st Fourier	100.0	96.4	99.8	99.8	95.3
2nd Fourier	96.4	100.0	97.0	97.0	94.8
Gauss	99.8	97.0	100.0	99.9	95.8
Voigt	99.8	97.0	99.9	100.0	95.8
M-E LOS field	95.3	94.8	95.8	95.8	100

In the sunspot, the 2nd Fourier-coefficient MDI-like algorithm behaves differently than the other algorithms, sometimes returning large negative velocities where the others return positive ones (e.g., at $x = 15$ Mm on the left panel of Figure 4, the 2nd-Fourier coefficients return $v_2 \approx -400$ m s^{-1} while the 1st-Fourier coefficients return $v \approx +150$ m s^{-1}), and vice-versa. In the penumbra especially, the 2nd Fourier-coefficients velocities are strikingly different from those returned by the 1st Fourier coefficients and the least-squares fits. Figure 5 shows the velocity maps obtained with the two MDI-like algorithms, confirming the discrepancy.

The algorithms ability to retrieve a correct velocity was tested by simulating Doppler shifts: LCP Fe I line profiles were selected at 3 different pixel locations (in the quiet Sun, in the penumbra, and in the umbra; see Figure 6), and were shifted in wavelength to replicate the impact of a Doppler velocity. The observables algorithms were then applied to the intensities derived from these shifted lines. The result is shown on Figure 7 (notice the different scale on the upper panel). In the quiet Sun and in the velocity range $[-5, +5]$ km s^{-1}, the four algorithms behave similarly and the difference between the retrieved velocity and the actual one (i.e. the error on velocity) does not vary much (the 2nd-Fourier coefficients algorithm displays the largest variation, ≈ 75 m s^{-1}). The offsets between the curves may reflect the difference in sensitivity to various parts of the Fe I line. The initial guess for the least-squares fits is provided by the 1st Fourier-coefficients MDI-like algorithm: if a zero velocity is used instead, the fits do not converge for velocities larger than ≈ 3.5 km s^{-1} (in absolute value). In the penumbra and umbra, the 1st Fourier-coefficients algorithm and the least-squares

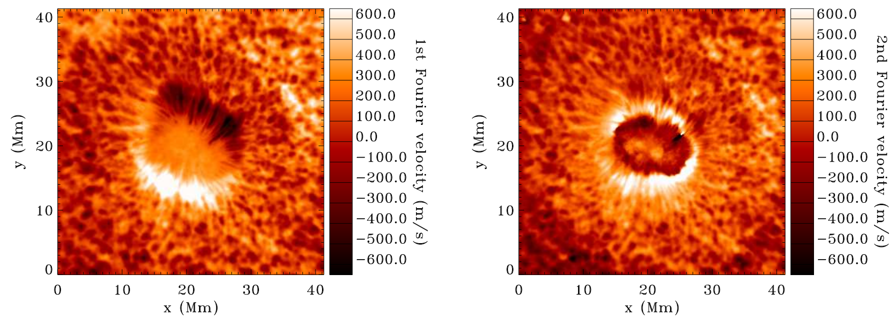

Figure 5. Doppler velocities returned by the MDI-like algorithm using the 1st (left panel) or 2nd (right panel) Fourier coefficients.

fits behave similarly in the velocity range $\approx [-5, +5]$ km s^{-1}. The 2nd Fourier-coefficients algorithm behaves differently and shows a larger dependence on input velocity. Moreover, the velocity error is significantly different in the umbra and penumbra. The 2nd-Fourier coefficients algorithm fares poorly compared to the other algorithms.

The standard deviation of Doppler velocity resulting from photon noise was computed in the quiet-Sun pixel for the different LOS algorithms, assuming an exposure time long enough to fill the HMI CCD well (i.e. an exposure level of 175000 photons): the results are listed in Table 2. The standard deviations of the least-squares fits are smaller than those of the MDI-like algorithms. The 2nd Fourier-coefficients algorithm has the largest standard deviation. Noticeably, an unweighted average of the velocities returned by the two MDI-like algorithms will only lower the standard deviation by less than 10% (and not $\sqrt{2}$ as might have been expected) compared to the 1st-Fourier coefficients alone.

Table 3 lists the correlation coefficients between LOS magnetic-field strengths. In this table and in the rest of the paper, M-E LOS field refers to the field strength inverted by the Milne-Eddington code and multiplied by the cosine of the field inclination angle Φ (relative to the vertical direction). The lowest correlation is obtained between 2nd Fourier-coefficients MDI-like algorithm and M-E inversion. In the sunspot umbra, the LOS magnetic-field strength returned by a_2 and b_2 is very different from the other algorithms (see Figure 4).

Even though we compare field strengths returned by various algorithms to the M-E inversion (used as a reference), it must be kept in mind that the Milne-Eddington atmosphere model is only approximate. In particular the atmospheric parameters are assumed to be height-independent, which is contradicted by the C-shape of the Fe I line bisector. The magnetic-field inclination angle and strength also vary with height. Therefore the observables algorithms are not expected to match the M-E results or to each return the same LOS field strengths, because of their different atmospheric-height sensitivities.

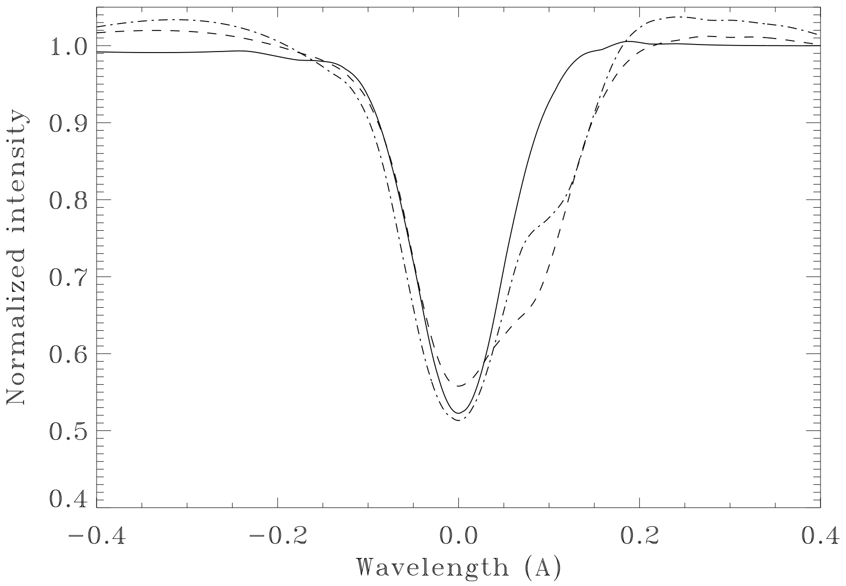

Figure 6. Comparison of Fe I line profiles from temporally-averaged wavelength-interpolated IBIS data: the solid line is from a quiet-Sun pixel, the dashed line is from a penumbral pixel, and the dash-dotted line is from an umbral pixel. The profiles are normalized by their respective continuum intensity.

Figure 8 shows the impact of the M-E field inclination angle Φ on the relative error in LOS field strength made by each algorithm. This relative error is the strength returned by an algorithm minus the M-E LOS field strength, divided by the M-E strength. For the 1st Fourier-coefficients MDI-like algorithm and least-squares fits, this error, at first, decreases (in absolute value) when the inclination angle increases from 0 to ≈ 35 degrees (corresponding to the sunspot umbra), it is relatively stable and small for Φ in the range $\approx 35-60$ degrees (corresponding to the inner penumbra), and then it increases steeply for $\Phi \gtrapprox 65$ degrees (outer penumbra). On this plot, only the pixels with an absolute field strength > 150 Gauss and located inside the square window of Figure 2 are shown, thus avoiding the noisiest values. The errors on the M-E inverted field strength and on Φ increase with Φ, which could explain the increase in relative error on the field strength for $\Phi \gtrapprox 65$ degrees. Overall, this relative error seems lower (in absolute value) in the sunspot penumbra than in the umbra.

None of the observables algorithm shows any dependence to the azimuth angle of the magnetic field.

Figure 9 shows the impact of Φ on the difference in Doppler velocity with the line-core velocity. The absolute value of this difference does not matter much as different algorithms are sensitive to different heights in the solar atmosphere: what matters is the dependence of this difference on the inclination angle. The 1st Fourier-coefficients MDI-like algorithm and the least-squares fit behave in a similar fashion: the difference in velocity slightly increases, in absolute value,

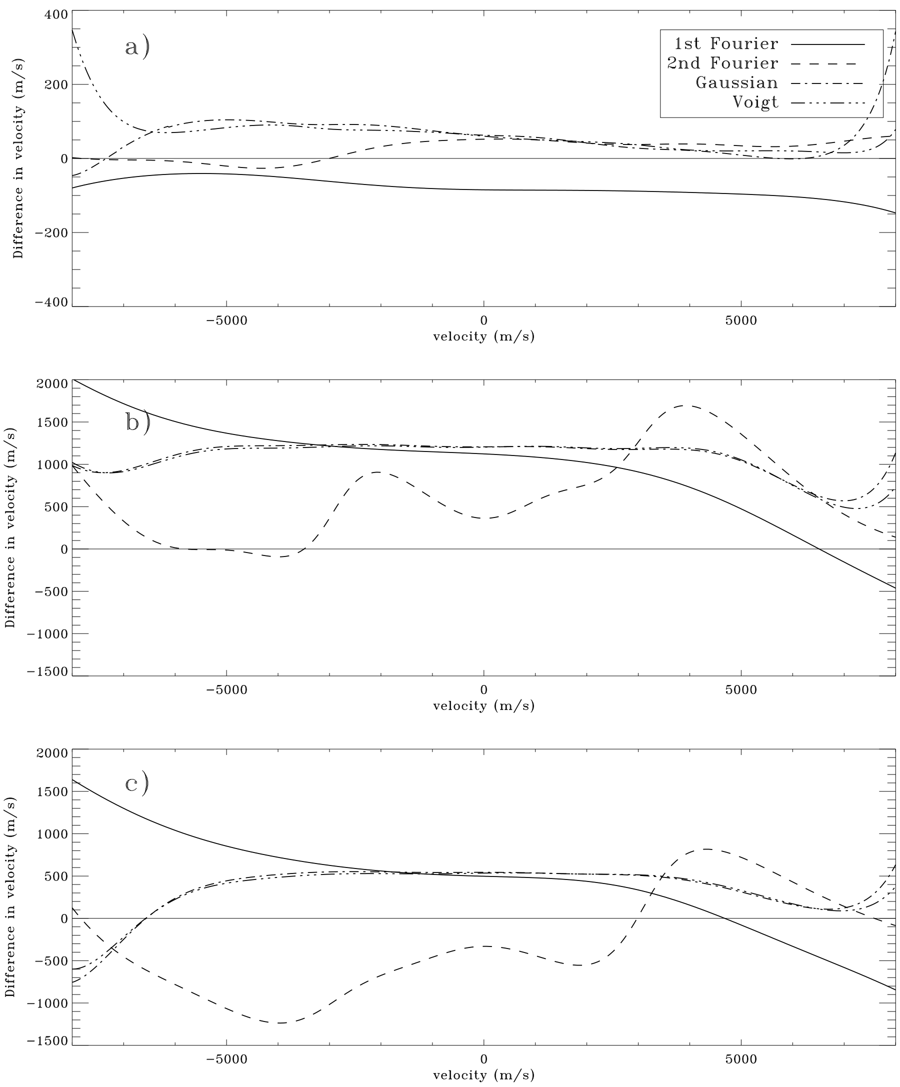

Figure 7. Difference in Doppler velocity retrieved by different algorithms and the input velocity v_{in}, as a function of v_{in}. Solid line: 1st Fourier-coefficients MDI-like algorithm; dashed line: 2nd Fourier-coefficients MDI-like algorithm; dash-dotted line: least-squares fit with a Gaussian profile; dash-dot-dot-dotted line: least-squares fit with a Voigt profile. a) for a quiet-Sun pixel; b) for a penumbral pixel; c) for an umbral pixel. The scale on the upper panel differs from the one on the other panels.

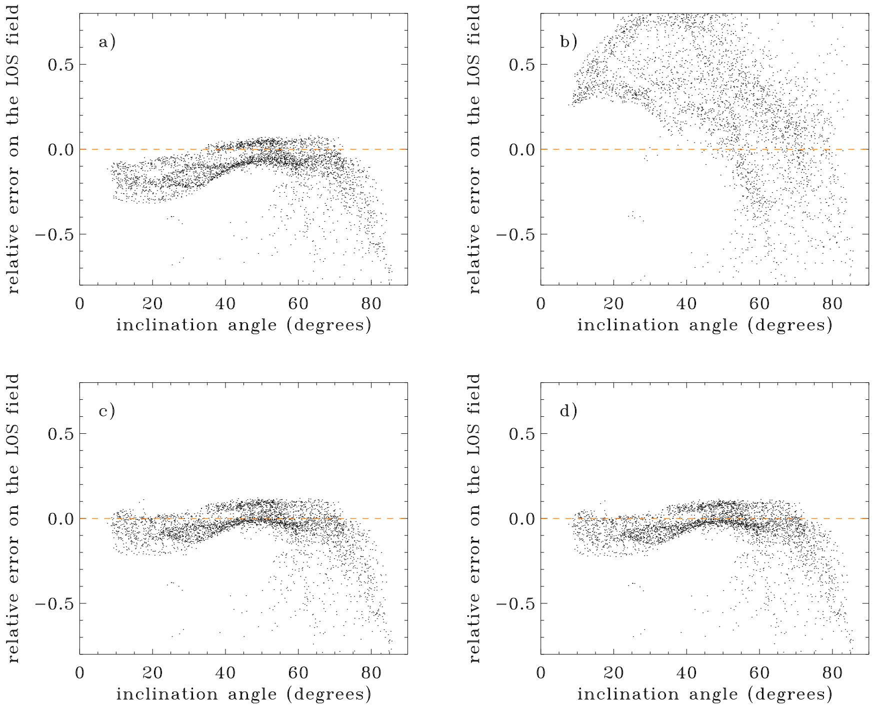

Figure 8. Ratio of the difference between LOS magnetic-field strength returned by the observables algorithms and M-E LOS field strength to the M-E LOS field strength, as a function of the field inclination angle Φ. a) MDI-like algorithm with 1st Fourier coefficients; b) MDI-like algorithm with 2nd Fourier coefficients; c) least-squares fit with a Voigt profile; d) least-squares fit with a Gaussian profile. Only the pixels with an absolute field strength > 150 Gauss and located inside the square window of Figure 2 are shown.

with Φ in the range $\approx 0-60$ degrees, and then it changes steeply. The MDI-like algorithm with 2nd Fourier coefficients behaves differently and shows a larger dispersion in velocity difference. In absolute value, these differences are larger in the sunspot inner penumbra than in the umbra.

On Figure 10, the fields weaker (in absolute value) than 1250 G (black dots) are isolated from stronger fields (orange dots). The Doppler-velocity scatter plots show almost separate orange and black branches: the relation between the velocities returned by the four algorithms and the line-core velocities depends on the field strength. Different field strengths may correspond to different parts of the sunspot. As previously observed, the 1st Fourier-coefficients MDI-like, Gaussian least-squares, and Voigt least-squares algorithms behave similarly, unlike the 2nd Fourier-coefficients algorithm which returns spurious velocities in regions of strong fields. Indeed, the orange branch of the upper right panel of Figure 10 is nearly vertical, and differs greatly from the black branch. Figure 11 shows scatter plots of the LOS field strength, and the lower right panel highlights how similar the values returned by the two least-squares fits are.

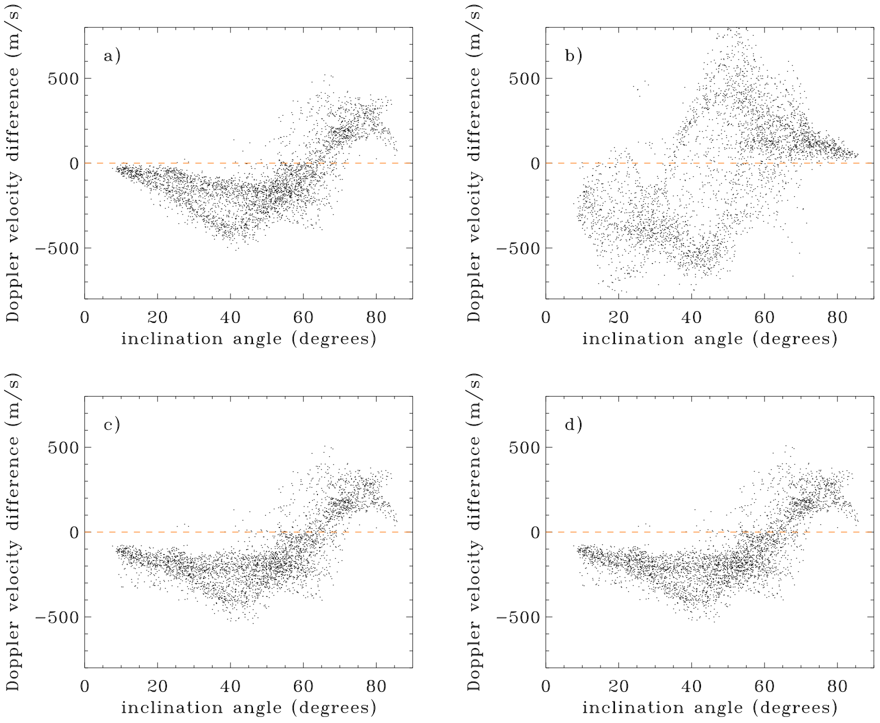

Figure 9. Differences in Doppler velocity returned by the observables algorithms with line–core velocity, as a function of the field inclination angle Φ. a) MDI-like algorithm with 1st Fourier coefficients; b) MDI-like algorithm with 2nd Fourier coefficients; c) least-squares fit with a Voigt profile; d) least-squares fit with a Gaussian profile. Only the pixels with an absolute field strength > 150 Gauss and located inside the square window of Figure 2 are shown.

Even though the previous results are presented as if the impacts of field strength and inclination angle were separable, these two quantities are related in a sunspot: strong fields — mostly located in the umbra and stronger than 1600 G in absolute value — have small inclinations ($\Phi \lessapprox 35$ degrees), while weaker fields — mostly in the penumbra — have large inclinations. Another consideration affecting the results is that the geometric height in the atmosphere where the Doppler signal is formed is not the same above the quiet Sun and above a sunspot.

Overall, least-squares fits perform better than the 1st Fourier-coefficients MDI-like algorithm in presence of a magnetic field, while the 2nd Fourier coefficients algorithm appears to be the least accurate algorithm. a_2 and b_2 are very sensitive to the Fe I line shape, much more so than a_1 and b_1. The deformation affecting the I+V and I−V components in presence of a strong and inclined field (see the I+V components on Figure 6) is not reflected in the look-up tables obtained from a line at rest. This explains the difficulties encountered during the commissioning phase of SDO when trying to use a_2 and b_2. The other algorithms tested are more robust in presence of a field.

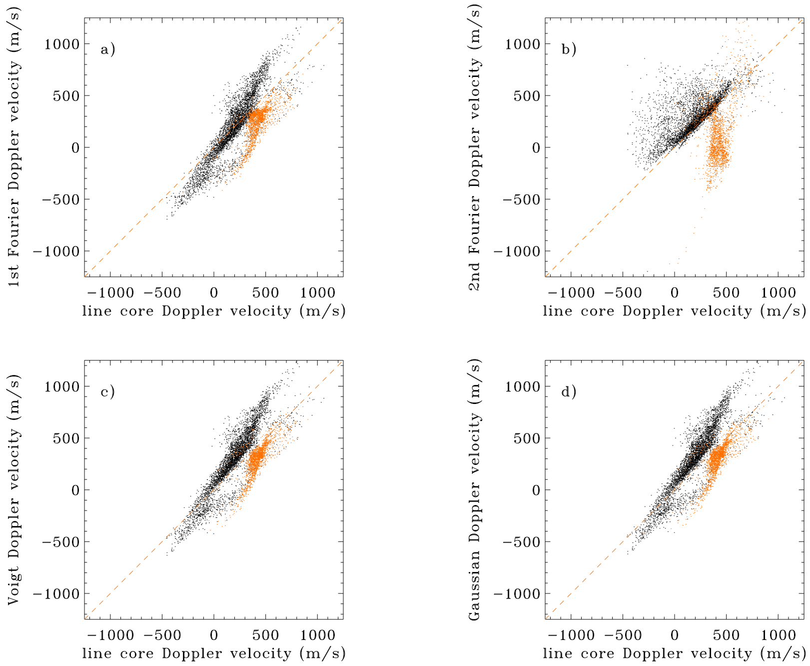

Figure 10. Scatter plots of the Doppler velocities returned by different algorithms with the line-core velocity. a) 1st Fourier-coefficient MDI-like algorithm; b) 2nd Fourier-coefficient MDI-like algorithm; c) least-squares fit with a Voigt profile; d) least-squares fit with a Gaussian profile. Black dots: absolute magnetic field strength < 1250 G; orange dots: absolute magnetic field strength > 1250 G.

Averaging Doppler velocities and magnetic-field strengths obtained from 1st and 2nd Fourier coefficients might not be beneficial to these observables: in the quiet Sun it will reduce the noise level due to photon noise (although by a factor smaller than $\sqrt{2}$) and may improve the accuracy of the results, but it is likely to degrade it in presence of strong magnetic fields.

Measurements based on the data of Figure 8 show that the 1st Fourier-coefficient MDI-like algorithm underestimates (in absolute value) the LOS field strength in a sunspot umbra (here defined as $\Phi < 35$ degrees) by an average value of $\approx 17\%$. Conversely, the 2nd Fourier-coefficients MDI-like algorithm overestimates this field strength, by more than 50% for many pixels. The least-squares fit (with a Gaussian or Voigt profile) provides more accurate results, but still underestimates the actual LOS field strength in the umbra (by $7-8\%$ on average). The use of a Voigt profile does not seem to improve the determination of the LOS observables compared to a simpler Gaussian. The implementation of the Voigt profile makes linedepth and linewidth sligthly more difficult to determine than with a basic Gaussian, because these quantities must be calculated from the fitted quantities I_d and σ (with a relation depending on the damping parameter a).

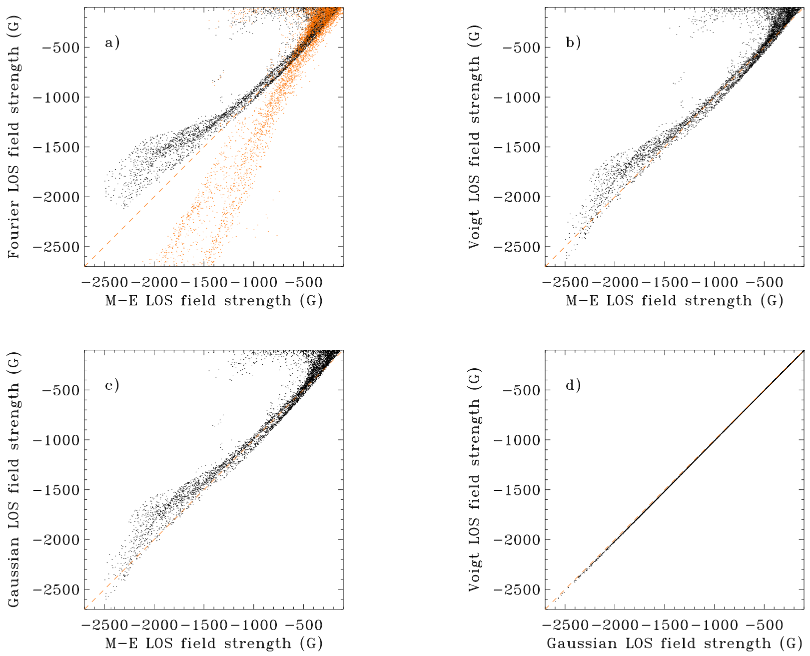

Figure 11. Scatter plots of LOS magnetic-field strengths returned by different algorithms with LOS field strength returned by the M-E inversion. a) 1st (in black) and 2nd (in orange) Fourier-coefficients MDI-like algorithm; b) least-squares fit with a Voigt profile; c) least-squares fit with a Gaussian profile; d) scatter between least-squares fits with a Voigt and Gaussian profile.

5.2. Other observables quantities: linewidth, linedepth, and continuum intensity

With IBIS data, linewidth, linedepth, and continuum intensity returned by observables algorithms can be compared to those quantities measured from the wavelength-interpolated line profiles (with a fine enough wavelength grid). The measured continuum intensity is the intensity of the Fe I profile at a wavelength λ far enough from line center (we selected $\lambda = -0.63$ Å). Figure 12 is a collection of scatter plots of the linewidth returned by different algorithms, while Figure 13 shows the linedepth, and Figure 14 shows the continuum intensity. On these three figures, the pixels with a M-E inclination angle $\Phi < 35°$ (roughly corresponding to the umbra) are separated from those with a more inclined field on the left panels, and the pixels with a field weaker than 1250 G (in absolute value) are separated from those with a stronger field on the right panels. The measured quantities are directly obtained from the interpolated IBIS profiles: the LCP and RCP components are processed separately and their values averaged. For the algorithms tested, the dispersion on the linewidth relative error (see Figure 15) increases with the magnetic-field strength and for less inclined fields: the linewidths returned are less robust in the sunspot umbra than in the penumbra and the quiet Sun. Linedepth (see Figure 16) and continuum-intensity relative

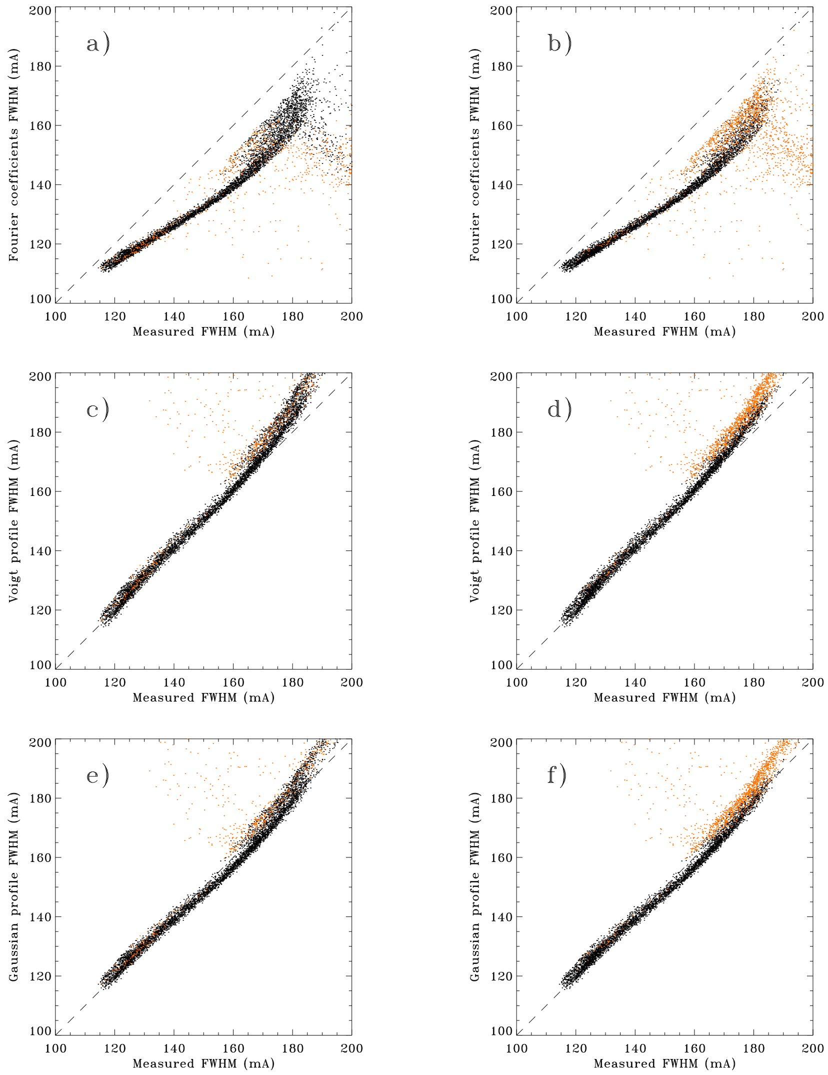

Figure 12. Scatter plots of FWHMs returned by different algorithms with actual (measured) FWHMs. a) and b) MDI-like algorithm; c) and d) least-squares fit with a Voigt profile; e) and f) least-squares fit with a Gaussian profile; a), c), and e) the black dots show pixels for which the magnetic field inclination is larger than 35°, while the orange dots are for less inclined fields; b), d), and f) the black dots show pixels for which the absolute magnetic field strength is < 1250 G, while orange dots are for stronger fields.

errors also show an increase in their dispersion with the field strength. The average relative errors on the linewidth are larger for strong fields (here we considered fields > 1600 G in absolute value). Again, the MDI-like algorithm (using both 1st and 2nd Fourier coefficients for these quantities) fares relatively poorly in presence of a magnetic field: it significantly underestimates the linewidth in the

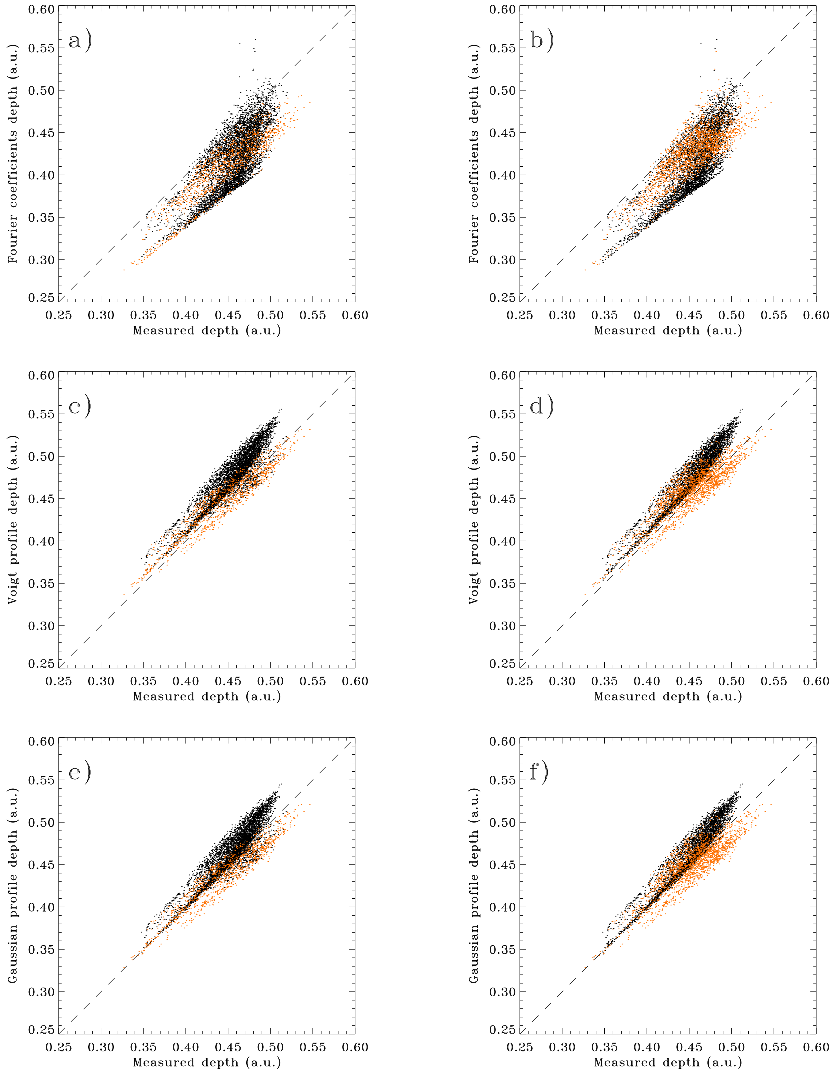

Figure 13. Scatter plots of linedepths returned by different algorithms with actual (measured) linedepths. a) and b) MDI-like algorithm; c) and d) least-squares fit with a Voigt profile; e) and f) least-squares fit with a Gaussian profile. a), c), and e) the black dots show pixels for which the magnetic field inclination is larger than 35°, while the orange dots are for less inclined fields; b), d), and f) the black dots show pixels for which the absolute magnetic field strength is < 1250 G, while orange dots are for stronger fields.

sunspot umbra and penumbra (by an average of $\approx 17.5\%$ for strengths > 1600 G in absolute value). As already mentioned, a strong and inclined field distorts the Fe I line. With Zeeman splitting, the σ components of a longitudinal field are contaminated by the π component when Φ is different from 0: the resulting profiles are different from the Gaussian assumed when deriving Eqs (6) and (7). The MDI-like algorithm also underestimates, by an average of $\approx 3.9\%$, the actual

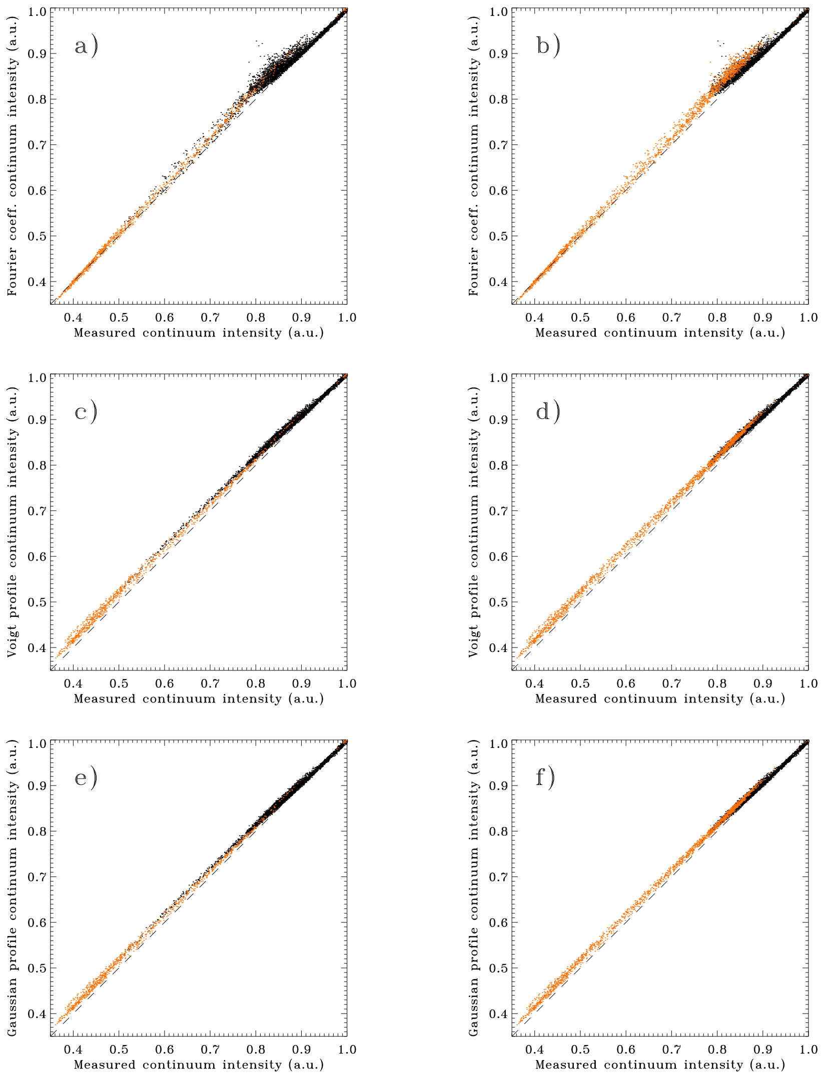

Figure 14. Scatter plots of (normalized) continuum intensities returned by different algorithms with actual (measured) continuum intensities. a) and b) MDI-like algorithm; c) and d) least-squares fit with a Voigt profile; e) and f) least-squares fit with a Gaussian profile. a), c), and e) the black dots show pixels for which the magnetic field inclination is larger than 35°, while the orange dots are for less inclined fields; b), d), and f) the black dots show pixels for which the absolute magnetic field strength is $<$ 1250 G, while orange dots are for stronger fields.

linewidth in the quiet Sun: even in absence of field the Fe I line is not a Gaussian and is asymmetrical. Therefore, the factor K_1 could be revised upward. Least-squares fits provide more robust linewidth and linedepth (smaller dispersion in their relative errors). Surprisingly, it appears that with the MDI-like algorithm the average relative error on linedepth is lower for stronger magnetic fields than for weaker ones. If only quiet Sun pixels are selected (e.g. fields weaker than 50 G in absolute value), the MDI-like algorithm underestimates the actual linedepth by $\approx 16\%$ (see Figure 16). This is after I_d returned by Equation (6) has been multiplied by K_2: this factor could also be revised upward. For stronger fields (> 1000 G in absolute value), the relative error on linedepth returned by the MDI-like algorithm is smaller ($\leq 11.5\%$ on average), and for a few pixels is even zero. This is unlike the least-squares fits for which the relative error on linedepth goes both ways in presence of stronger fields and is $\leq 3.8\%$ on average in absolute value. In the quiet Sun, the least-squares fits overestimate the linedepth by $< 2.8\%$ on average.

The continuum intensity obtained from the MDI-like algorithm is slightly underestimated by $\approx 1.7\%$ on average in the quiet Sun, while the least-squares fit with a Voigt profile overestimates the intensity in the quiet Sun by $\approx 0.7\%$, and the least-squares fit with a Gaussian underestimates it by 0.15% on average. On Figure 14, the slopes of the curves are different for stronger and weaker fields and for smaller and larger inclination angles, with the MDI-like algorithm. Such an effect seems absent with the least-squares fits.

6. Conclusion

Spectropolarimetric images of the solar surface obtained by the IBIS instrument were used to investigate the accuracy of LOS observables returned by the MDI-like algorithm implemented in the processing pipeline of the SDO/HMI instrument. Three other observables algorithms were also tested: a MDI-like algorithm based on the 2nd Fourier coefficients, a least-squares fit with a Gaussian profile, and a least-squares fit with a Voigt profile. In presence of magnetic fields, the least-squares fits are more accurate than the MDI-like algorithms (as expected). The 2nd Fourier-coefficient MDI-like algorithm fares especially poorly in a sunspot, probably due to the significant distortion of the I+V and I−V Stokes profiles in strong and inclined magnetic fields compared to the line at rest. A contrived way of improving the MDI-like algorithm would be to implement different look-up tables, depending on the variation of a reference Fe I line model with magnetic field strength and inclination, and to use these tables in presence of a magnetic field. Alternatively, a weighting scheme could be used to combine 1st and 2nd Fourier-coefficients results, and to reduce the impact of 2nd Fourier coefficients in strong fields. Combining 1st and 2nd Fourier-coefficients results for Doppler velocity and LOS field strength is appealing in the quiet Sun to reduce the noise level due to photon noise (although by a factor smaller than might be expected), but it will likely degrade the accuracy of the LOS observables in strong magnetic fields. It is probably better to drop the MDI-like method altogether in favor of a least-squares fit. A major issue is the computation speed:

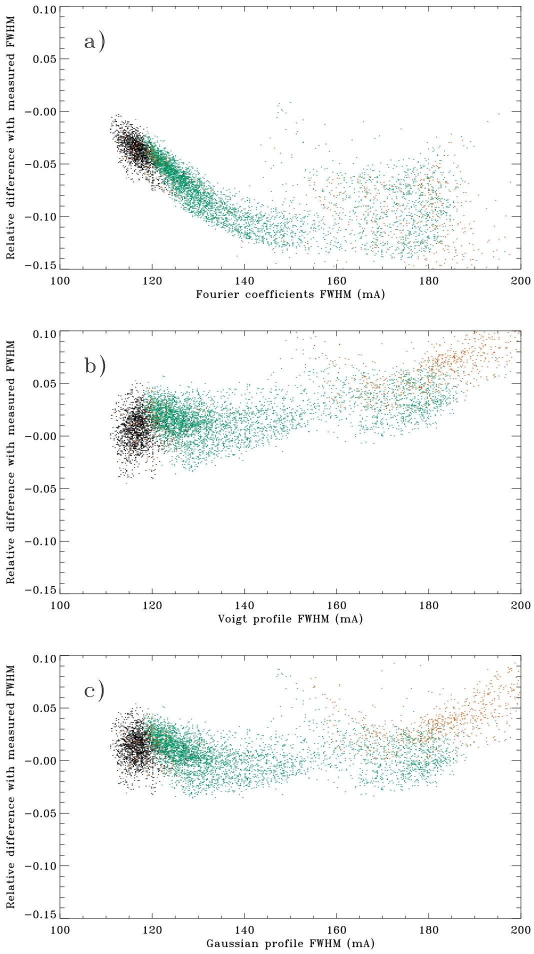

Figure 15. Relative difference in the FWHMs returned by different algorithms with the actual (measured) FWHMs. a) MDI-like algorithm; b) least-squares fit with a Voigt profile; c) least-squares fit with a Gaussian profile. The black dots show pixels for which the absolute magnetic field strength is < 50 G, while orange dots are for fields > 1600 G, and green dots are for fields in the range $1000 - 1600$ G.

least-squares fits are much slower than the MDI-like algorithm, and their initial guess must be provided by another algorithm. Moreover, least-squares fits might not always converge: in the study on temporally-averaged IBIS data this was an issue only when the initial Doppler velocity guess was set to zero. In that case we encountered non-convergences for a few pixels inside the sunspot. When the initial guess was set to the result of the MDI-like algorithm, the fits converged for all pixels. In the study of simulated Doppler velocities based on three different line profiles (one from an umbral pixel, one from a penumbral pixel, and one from a quiet Sun pixel), we had non-convergences — despite using the appropriate initial guess — only 0.5% of the time and for very large Doppler velocities

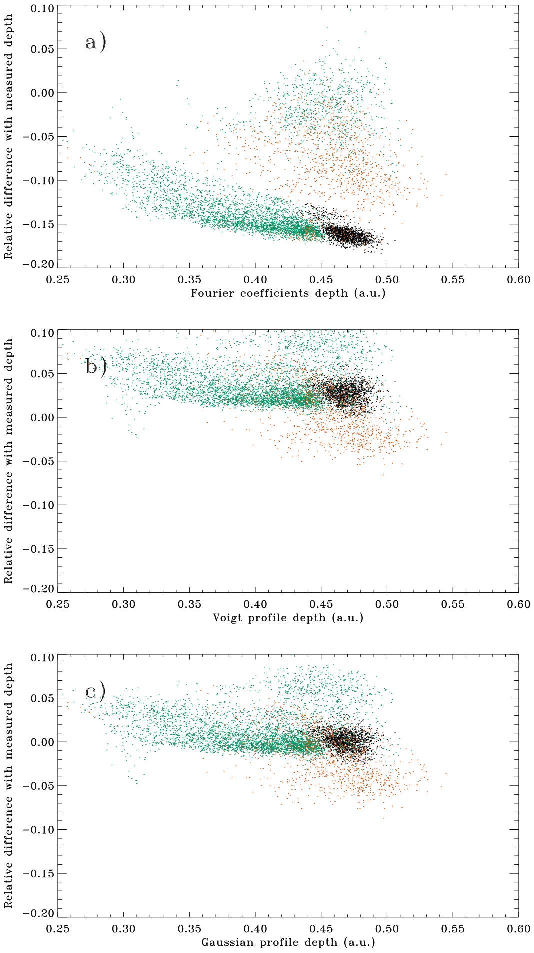

Figure 16. Relative difference in the linedepths returned by different algorithms with the actual (measured) linedepths. a) MDI-like algorithm; b) least-squares fit with a Voigt profile; c) least-squares fit with a Gaussian profile. The black dots show pixels for which the absolute magnetic field strength is < 50 G, while orange dots are for fields > 1600 G, and green dots are for fields in the range $1000 - 1600$ G.

(> 8500 m s^{-1}). Therefore, in the case of a strong sunspot observed by HMI far from solar disk center and at a large Sun-SDO radial velocity, it is quite possible that a least-squares fit does not converge for some pixels.

In the quiet Sun at least, the noise level on Doppler velocities due to photon noise is lower with least-squares fits than with MDI-like algorithms.

Overall, the (1st Fourier-coefficients) MDI-like algorithm performs relatively well even in presence of a strong field. Linewidths, linedepths, and LOS magnetic field strengths (in absolute value) are underestimated in the sunspot. The linewidth is underestimated by $\approx 3.9\%$ in the quiet Sun, and by an average $\approx 17.5\%$ in the sunspot where the field is stronger than 1600 G (in absolute value). The linedepth is underestimated by $\approx 16\%$ in the quiet Sun, and by less in the sunspot. The continuum intensity is only slightly underestimated by $1-1.7\%$. The absolute value of the LOS field strength is underestimated by an average of $\approx 17\%$ in the sunspot umbra. Finally, the Doppler velocities returned by the 1st Fourier-coefficients algorithm and the least-squares fits differ by about 90 m s^{-1} (on average) in the sunspot umbra, with a peak difference of ≈ 300 m s^{-1}, after the respective average velocities in the quiet Sun are subtracted from the results of each algorithm.

The results presented here make it possible to partly correct some LOS observables obtained with the current HMI pipeline. For instance, the K_1 and K_2 factors multiplying linewidth and linedepth could be revised upwards, and could be a function of the magnetic-field strength returned by the MDI-like algorithm. Since the IBIS data were taken prior to the SDO launch, it will be interesting to have simultaneous observations by HMI and IBIS, and to this end a proposal was submitted to — and accepted by — the National Solar Observatory. Finally, the Fe I line seen by IBIS is slightly different from the HMI one (both instruments have different spatial resolutions and scattered light levels), and the line profiles used here are convolved by the IBIS filter transmittances and are temporally averaged: therefore, the present results might be somewhat different from what the Fe I line seen by HMI would return.

Acknowledgements This work was supported by NASA Grant NAS5-02139 (HMI). The data used here are courtesy of NASA/SDO and the HMI science team. We thank the HMI team members for their hard work. We also thank professor R. Ulrich for providing us with Fe I line profiles from Mount Wilson Observatory.

References

Bell, B., Meltzer, A.: 1959, *Smithsonian Contribution to Astrophysics* **3**, 39.
Borrero, J.M., Tomczyk, S., Kubo, M., Socas-Navarro, H., Schou, J., Couvidat, S., Bogart, R.: 2010, *Solar Phys.* in press (DOI: 10.1007/s11207-010-9515-6).
Cavallini, F.: 2006, *Solar Phys.* **236**, 415.
Couvidat, S., Schou, J., Shine, R.A., Bush, R.I., Miles, J.W., Scherrer, P.H., Rairden, R.L.: 2011, *Solar Phys.* in press (DOI: 10.1007/s11207-011-9723-8).
Dravins, D., Lindegren, L., Nordlund, Å.: 1981, *Astron. Astrophys.* **96**, 345.
Norton, A.A., Graham, J.P., Ulrich, R.K., Schou, J., Tomczyk, S., Liu, Y., Lites, B.W., Ariste, A. Lopez, Bush, R.I., Socas-Navarro, H., Scherrer, P.H.: 2006, *Solar Phys.* **239**, 69.
Rajaguru, S.P., Wachter, R., Sankarasubramanian, K., Couvidat, S.: 2010, *ApJ* **721**, L86.
Scherrer, P.H., Bogart, R.S., Bush, R.I., Hoeksema, J.T., Kosovichev, A.G., Schou, J., *et al.*: 1995, *Solar Phys.* **162**, 129.
Schou, J., Scherrer, P.H., Bush, R.I., Wachter, R., Couvidat, S., Rabello-Soares, M.C., *et al.*: 2011, *Solar Phys.* submitted.
Skumanich, A., Lites, B.W.: 1987, *ApJ* **322**, 473.
Wachter, R., Schou, J., Rabello-Soares, M.C., Miles, J.W., Duvall, T.L., Jr., Bush, R. I.: 2011, *Solar Phys.* in press (DOI: 10.1007/s11207-011-9709-6).